Supplementary Information

Fluorescent and charge transport properties of columnar phases made of mono and bi-phenazine derivatives

J. Szydłowska, A. Sitkiewicz, E. Nazaruk, D. Pociecha, P. Krzyczkowska, A. Krówczyński and E. Gorecka

Experimental

Synthesis of materials

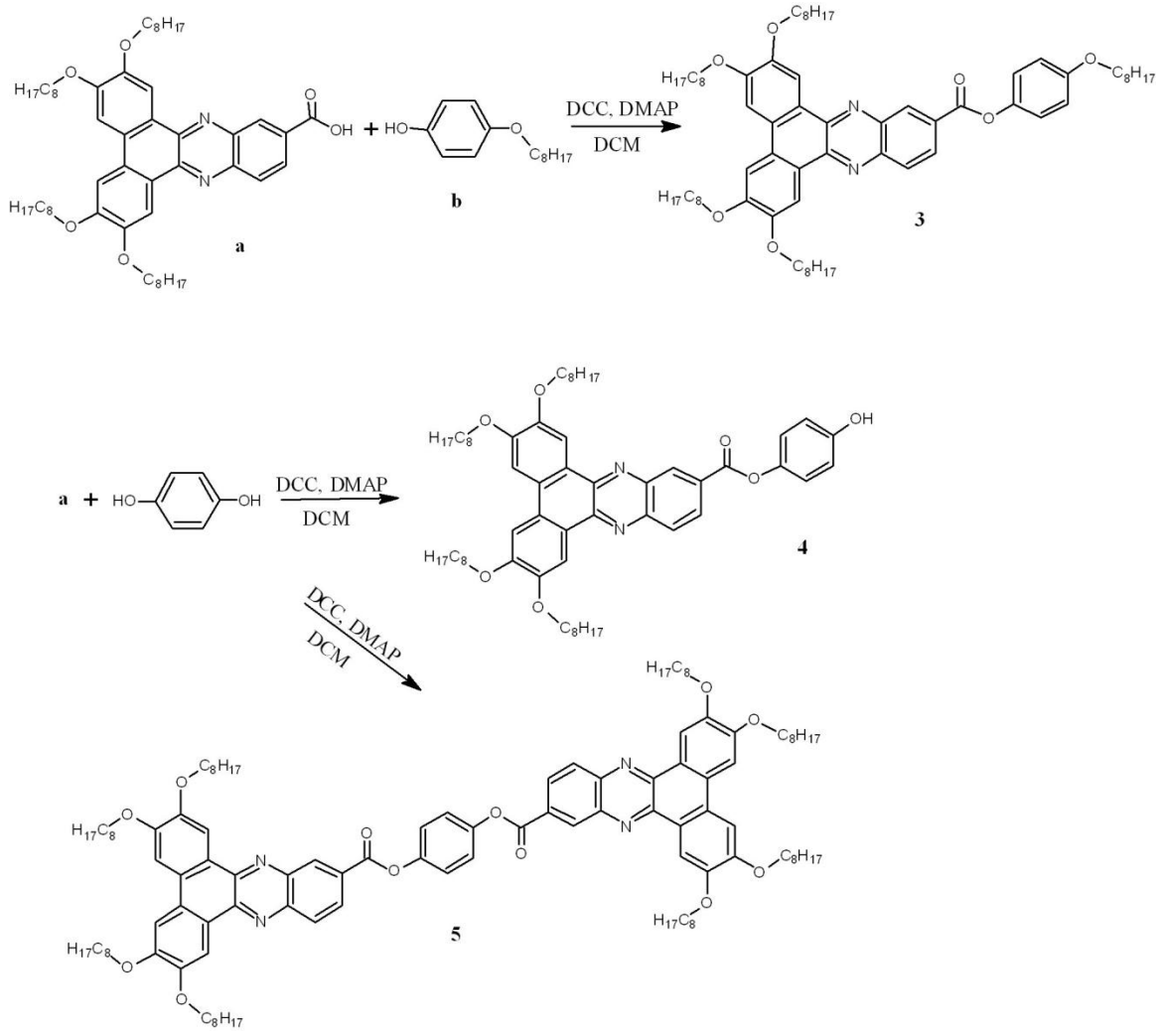

Scheme SI 1. Synthesis of compounds **3** – **5**.

Supplementary Information

Chemical procedures

The chemical procedures to synthesize the compounds **3** – **5** are as follows:

4-octyloxyphenyl-2,3,6,7-tetrakisoctyloxy-dibenzo[a,c]phenazine-11-carboxylate (**3**):

2,3,6,7-tetrakisoctyloxy-dibenzo[a,c]phenazine-11-carboxylic acid (**a,** prepared according to procedure described in Ref. 1) (0.83 g, 1.0 mmol), N,N-dicyclohexylcarbodiimide (**DCC**) (0.21 g, 1.0 mmol) and 4-(N,N-dimethyloamino) pyridine (**DMAP**) (0.025g, 0.2 mmol) were added to solution of 4-oktyloxyphenol (**b**) (0.222 g, 1.0 mmol) in dry methylene chloride (**DCM**) (20 ml). The mixture was stirred for 12 h at room temperature and then filtered. From the filtrate the solvent was evaporated and from the residue the compound **3** (620 mg) was separated in thin layer chromatography (CH_2Cl_2, silicagel). Yield: 61%.

Elemental analysis for $C_{67}H_{96}N_2O_7$ calculated: C 77.27; H 9,29; N 2.69; found: C 77.35; H 9,19; N 2.78;

^{1}*H NMR* (500 MHz, $CDCl_3$) 0.87-2.02 (m, 75H); 3.99 (t, 2H); 4.19-4.31 (m. 8H); 6.98 and 7.29 (AA', BB', J=9.1 Hz, 4H); 7.53 (s, H); 7.543 (s, H); 8.26 (d, J=8.8 Hz, H); 8.43 (dd: J=1.9 Hz, J=8.8 Hz, H); 8.594 (s, H); 8.596 (s, H); 9.08 (d, J=1.9 Hz, H).

4-hydroxyphenyl 2,3,6,7-tetrakisoctyloxy-dibenzo[a,c]phenazine-11-carboxylate, mono-ester (**4**) and di-ester (**5**):

The material (**a**) (0.83 g, 1.0 mmol), N,N-dicyclohexylcarbodiimide (**DCC**) (0.23 g, 1.1 mmol) and 4-(N,N-dimethyloamino)pyridine (**DMAP**) (0.025g, 0.2 mmol) were added to solution of hydrochinone (0.083 g, 0.75 mmol) in dry methylene chloride (**DCM**) (50 ml). The amount of hydroquinone was less than stechiometric to allow to run two reaction channels. The mixture was stirred for 12 h at room temperature and then filtered. From the filtrate solvent was evaporated and from the residue the compounds (**4**) (0.27 g) and (**5**) (0.28 g) were separated in thin layer chromatography (CH_2Cl_2, silicagel). Yield: 60% and 65% respectively.

Compound **4**

Elemental analysis for $C_{59}H_{80}N_2O_7$ calculated C 76.26; H 8,68; N 3.01; found C 76.32; H 8,6;

^{1}*H NMR*, δH (500 MHz, $CDCl_3$) 0.86-2.02 (m, 60H); 4.25-4.31 (m, 4H); 4.32-4.37 (m,4H); 6.92 and 7.19 (AA', BB', J=9.0 Hz, 4H); 7.69 (s, 2H); 8.38 (d, J=8.8 Hz, H); 8.48 (dd: J=1.9 Hz, J=8.8 Hz, H); 8.76 (s, H); 8.77 (s, H); 9.20 (d, J=1.9 Hz, H).

Compound **5**

Elemental analysis for $C_{112}H_{154}N_4O_{12}$ calculated C 76.94; H 8.88; N 3.20; found C 76.82; H 8.80; N 3.24;

^{1}*H NMR**, δH (500 MHz, $CDCl_3$) 0.86-2.03 (m, 120H); 4.23-4.36 (m, 16H); 7.46 (s, 4H); 7.61 (s, 2H); 7.64 (s, 2H); 8.64 (d, j=8.8 Hz, 2 H); 8.48 (dd: J=1.9 Hz, J=8.8 Hz, 2H); 8.65 (s, 2H); 8.69 (s, 2H); 9.11 (d, J=1.9 Hz, 2H).

*the spectrum was recorded at 55 ^{o}C, at room temperature the NMR signals were very broad, probably due to monomer – oligomer equilibrium.

Identification of mesophases

The mesophases were identified on a basis of characteristic optical textures, using Zeiss Axio Imager A2m polarizing microscope equipped with a Linkam heating stage. The structure of liquid crystalline phases was confirmed in X-ray measurements performed for powder or partially aligned samples with Bruker D8 GADDS diffractometer (CuKα radiation, Geoble mirror monochromator, point collimator, Vantec 2000 area detector), equipped with modified Linkam heating stage. For small angle diffraction experiments Bruker NANOSTAR diffractometer was used (CuKα radiation, cross-coupled Geoble mirrors, 3-pin hole collimation setup, MRI-TCPU heating stage, Vantec 2000 area detector). Phase transition temperatures and enthalpy changes were determined by calorimetric measurements performed with a TA DSC Q200 set up in inert atmosphere. The phase transition temperatures were determined as an onset of peak tangential line.

Vis Spectroscopy

Absorption spectra were measured for diluted solutions ($3\text{-}5\cdot10^{-2}$ g·dm^{-3}) using Schimadzu PC3100 spectrometer, for emission spectra FluoroLog HORRIBA Jobin Ivon spectrometer was used. Solvents having different molecular dipole moments: toluene (tol) μ_{tol} = 0.36 D, methylene chloride (DCM) μ_{DCM} = 1.6 D, N-methyl-2-pyrrolidone μ_{NMP} = 4.1 D were applied. For emission spectra the sample was the excited with 430 nm wavelength. Fluorescence quantum yields were measured in methylene chloride using the standard method [2] taking fluorescein dissolved in 0.1 M NaOH as standard material. (fluoresceine quantum yield: Φ_{ref} = 0.79, refractive indices: n_{NaOH} = 1.335, n_{DCM} = 1.424; $\Phi = \Phi_{ref}\,(\mathrm{grad}/\mathrm{grad}_{ref})(n_{DCM}/n_{NaOH})^2$).

Cyclic voltametry

Cyclic voltammetry studies were carried out using the bipotentiostat (*CH* Instruments 750E, Austin, Tx, USA) in the three-electrode arrangements with Ag/AgCl as the reference electrode, platinum foil as the counter and glassy carbon electrode (GCE, BASi, *A*=0.070 cm^2) as the working electrode. 0.1M tetrabutylammonium hexafluorphosphate (TBAPF 6) in dichloromethane (DCM) was used as the supporting electrolyte. The analyzed samples were deoxygenated prior to measurements by purging

with argon (99.999 %) for 15 min and then argon was passed over the solution surface. At each measurement series the reference electrode potential was calibrated using ferrocene (Fc/Fc^+) in the same supporting electrolyte solution and the calibration constant E_{ferr} were found. The formal potentials were determined from cyclic voltammetry waves as averaged oxidation/reduction potential. When CV waves were not clearly shaped the square wave voltammetry was applied. The energies of HOMO/LUMO levels of a given compound (E_{HOMO} and E_{LUMO}) were evaluated from its first oxidation and the first reduction potentials. The energy E_{HOMO} and E_{LUMO} levels were calculated according to the following equations $E_{HOMO} = -(E_{ox} - E_{ferr} + 4.8)$ eV and $E_{LUMO} = -(E_{red} - E_{ferr} + 4.8)$ eV.

Time of flight method for charge mobility

The TOF experiment was performed in conventional setup, similar to those described in ref. [3]. All wire connections had grounded screens. The voltage applied to the sample was in the range of 25 – 115 V. The transient photocurrent was measured over 1 kΩ resistor and recorded with 300 MHz digitizing oscilloscope (Agilent Technologies DSO6034A) triggered by the laser pulse. The estimated response time of the whole setup was less than 500 ns. The measurements were performed in 10 μm thick cells having ITO electrodes covered with homogeneous surfactant, the cells were filled by the studied substances using capillary forces. Inside the cell a thin sheet of separated charges (holes and electrons) were generated by a short light pulse (355 nm wavelength, ~8 ns pulse width) coming from solid state laser EKSPLA NL202. To avoid a space charge effect the sample was illuminated by a single pulses. If for better registration a group of pulses was necessary a sequence of single pulses was manually generated to give the sample enough time for relaxation. To reduce a noise the final signal was averaged over 16 runs. When in a series of measurements non-dispersive photocurrent curves were registered the transition time τ was determined as the intersection of two lines tangential to the plateau and the tail. For some compounds the photocurrent-time plot was drawn in double logarithmic scale and the transition time τ was assigned to the time at which a slope of the curve rapidly changed.

X-ray studies

Table SI1. Crystallographic distances (in Å) corresponding to X-ray diffraction signals calculated parameters of crystallographic lattice, a (in Å); d_c and d_d – distance between chains and discs (in Å).

	T/ °C	Phase	signals/Å	a/Å	d_c/ Å	d_d/Å
1	114	Col_{hd}	19,8	22.9	4.6	-
2	155[p]	Col_{hd}	18.9; 10.9; 9.5; 10.9; 9.5	21.8	4.5	3.5
3	100	Col_{hd}	21.0; 12.2; 10.5	24.3	4.6	3.5
4	120	Col_{hd}	19.2; 11.1; 9.5	22.2	4.6	3.5
	35	Col_r	23.2; 19.5; 18.1; 11.0; 9.8	a=36.3[a]		
				b=23.2[a]		
5	166	Col_{hd}	18.7; 10.9; 9.4	21.9	4.7	3.5

[a]for rectangular crystallographic lattice

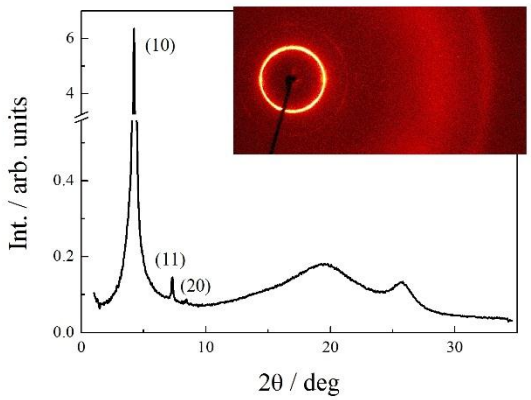

Figure SI1. XRD pattern of Col_{hd} phase of compound **4**. Low angle signals were indexed assuming 2D hexagonal lattice with unit cell size a = 22.2 A.

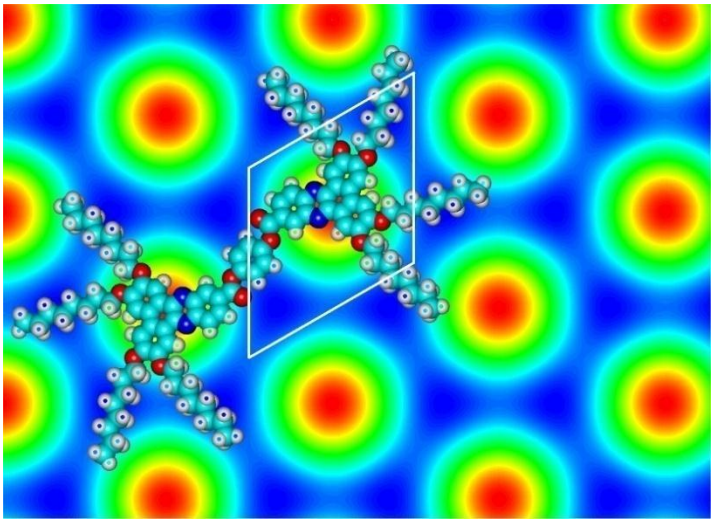

Figure SI2. Electron density map for Col_{hd} phase of compound **5**, obtained by reverse FT of the XRD pattern, all components in the Fourier series were taken as positive square root of the diffraction signal intensity. The arrangement of dimeric molecule in the lattice is shown, the cross-section of a single column is filled with half of the molecule

Absorption and emission

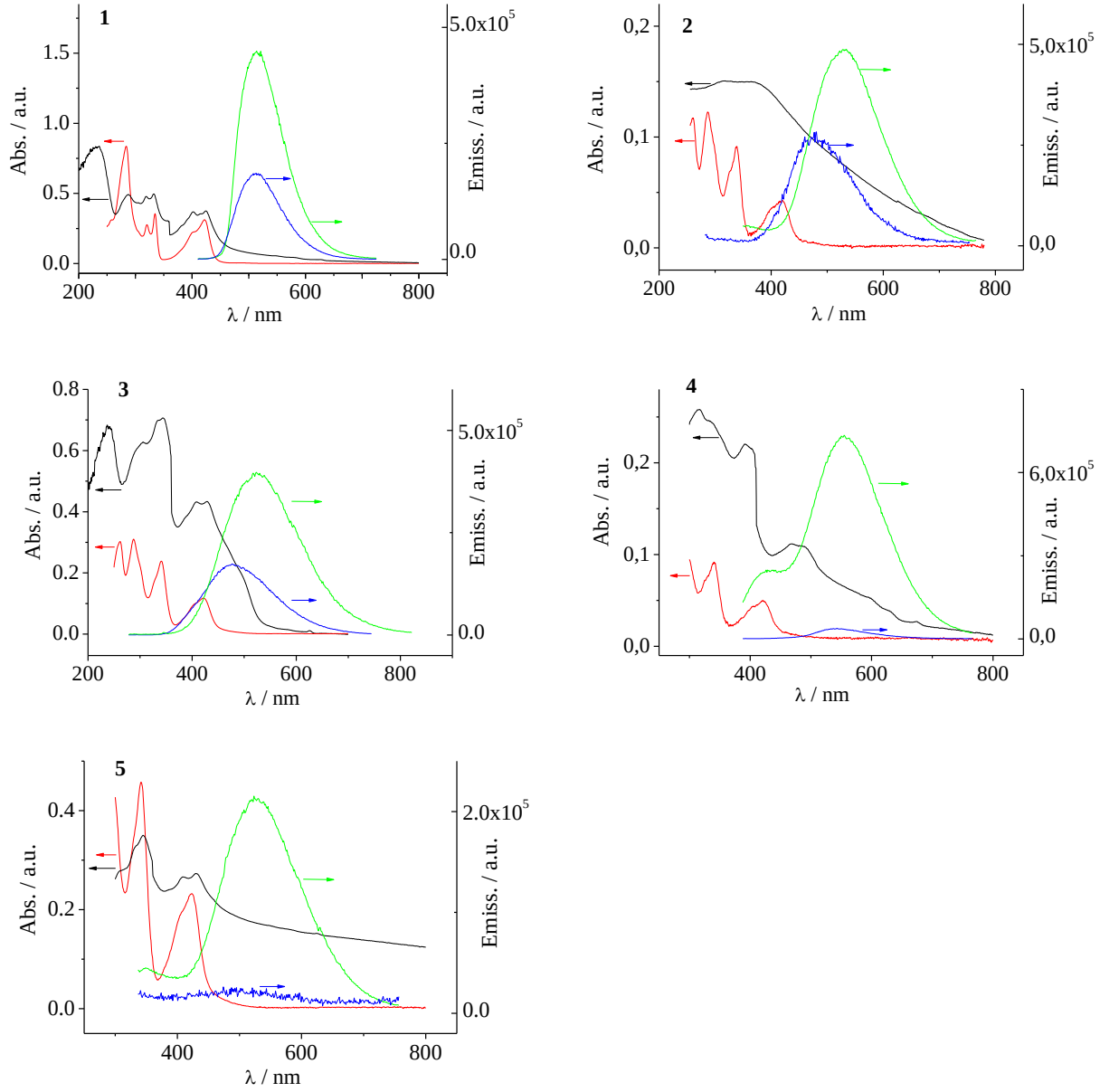

Figure SI3. Absorption and emission spectra of materials **1** – **5**; — abs. in solution of DCM, — abs. in solid state, — emission in solution of DCM, — emission in solid state.

Table SI2. Absorption peaks λ_{abs}^{sol} for compounds **1** – **5** in different solvents (tol – toluene, DCM – dichloromethane, NMP – N-methyl-2-pyrrolidone).

	λ_{abs}^{tol} nm	λ_{abs}^{DCM} nm	λ_{abs}^{NMP} nm
1	286 , 320, 334, 400, 422	284, 321, 334, 401, 422	285, 321, 335, 403, 426
2	287, 327, 340, 401, 421	261, 287, 338, 400, 420	262, 289, 341, 407, 425
3	287, 328, 342, 402, 424	261, 287, 341, 402, 422	264, 288, 343, 407, 427
4	288, 328, 342, 402, 423	260, 287, 341, 403, 421	262, 288, 342, 405, 427
5	288, 330, 342, 403, 425	261, 288, 342, 403,423	263, 289, 344, 424

Electrochemical studies

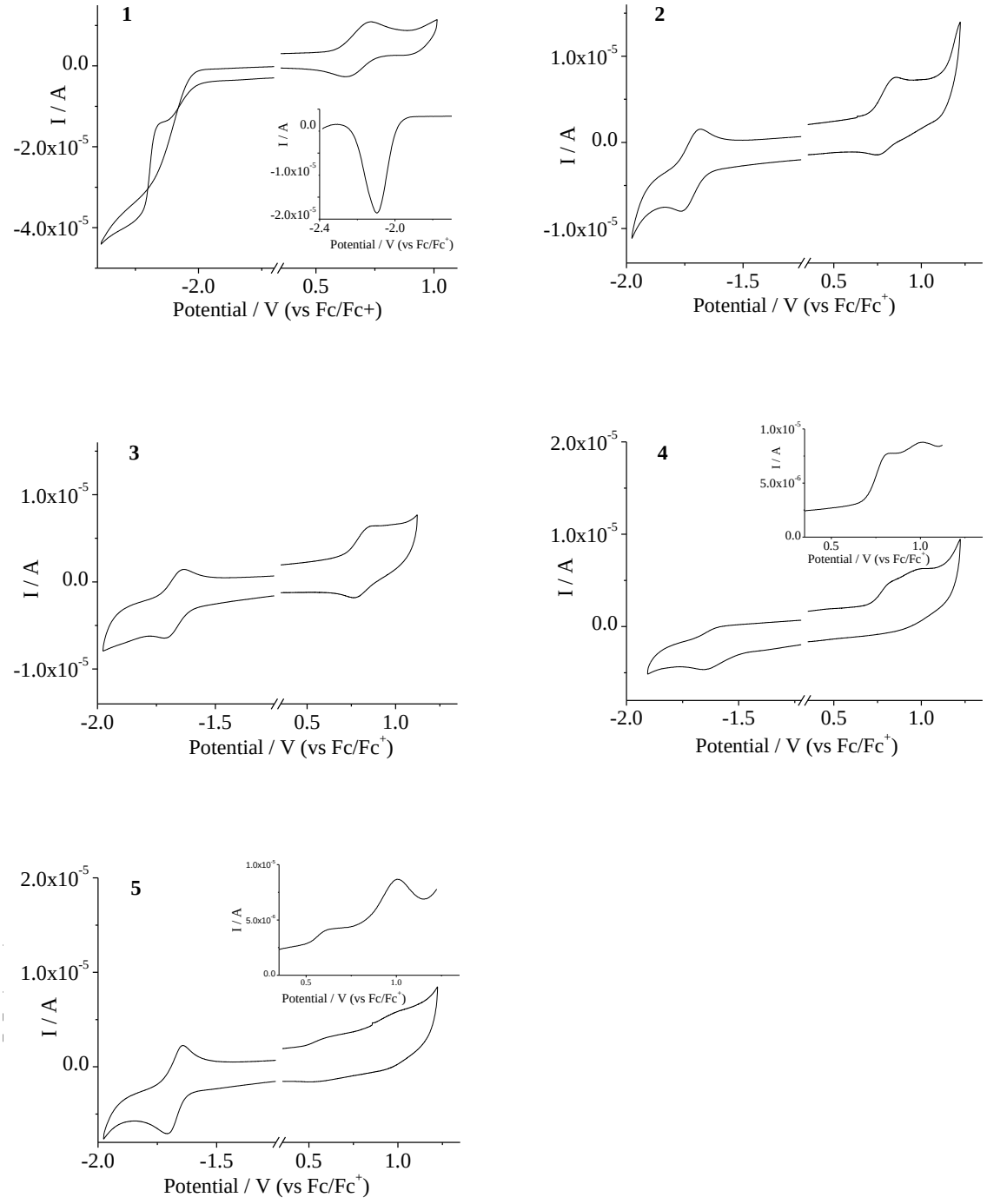

Figure SI4. Cyclic voltammograms for compounds **1** – **5** measured in dichloromethane and scaled *vs* ferrocene (Fc/Fc^+) potential; in insets – square wave voltammograms.

TOF studies

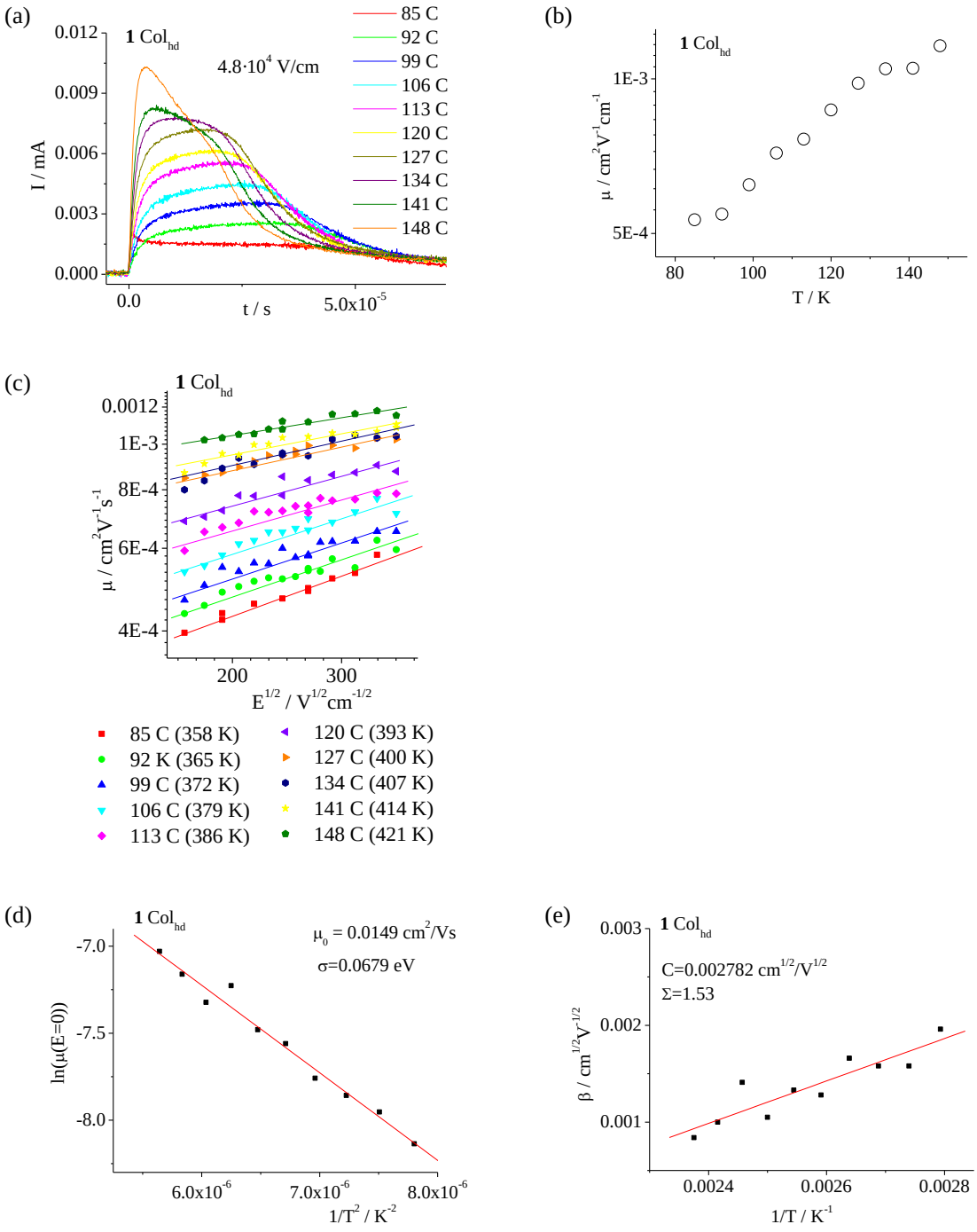

Figure SI5. Data compound **1:** (a) TOF transients current of holes at constant electric field (4.8 · 10^4 V/cm) in the temperature range of Col$_{hd}$ phase. (b) Temperature dependence of hole mobility at constant electric field (9.7 · 10^4 V/cm) in Col$_{hd}$ phase. (c) Field dependence of hole mobility (Poole-Frenkel relation) in Col$_{hd}$ phase. (d) Zero-field hole mobility and (e) slope β of the $\ln\mu(E^{1/2})$ dependence given in (c), $\beta = C[(\sigma/kT) - \Sigma]$.

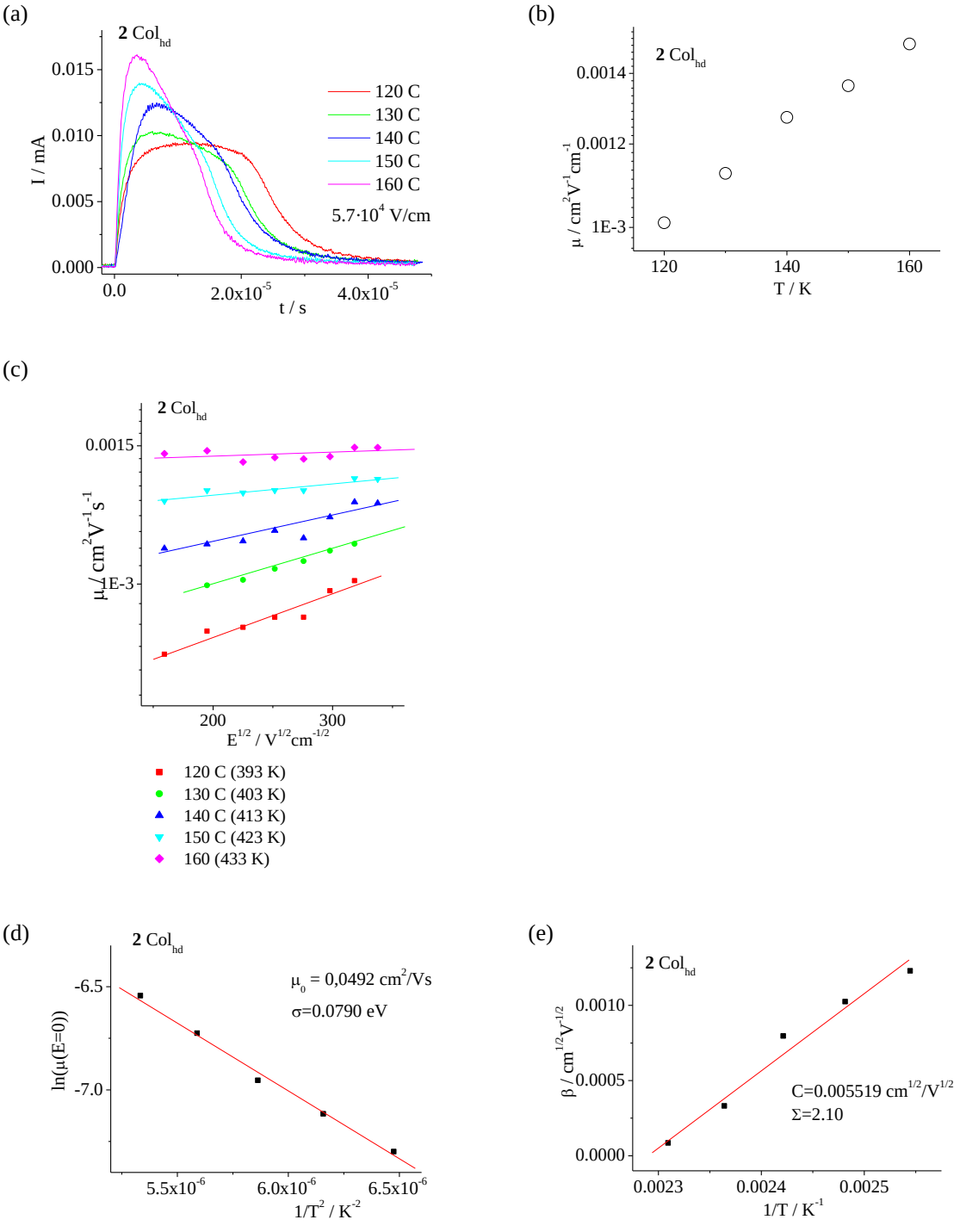

Figure SI6. Data compound **2:** (a) TOF transients current of holes at constant electric field ($5.7 \cdot 10^4$ V/cm) in the temperature range of Col_{hd} phase. (b) Temperature dependence of hole mobility at constant electric field ($9.7 \cdot 10^4$ V/cm) in Col_{hd} phase. (c) Field dependence of hole mobility (Poole-Frenkel relation) in Col_{hd} phase. (d) Zero-field hole mobility and (e) slope β of the $\ln\mu(E^{1/2})$ dependence given in (c), $\beta = C[(\sigma/kT) - \Sigma]$.

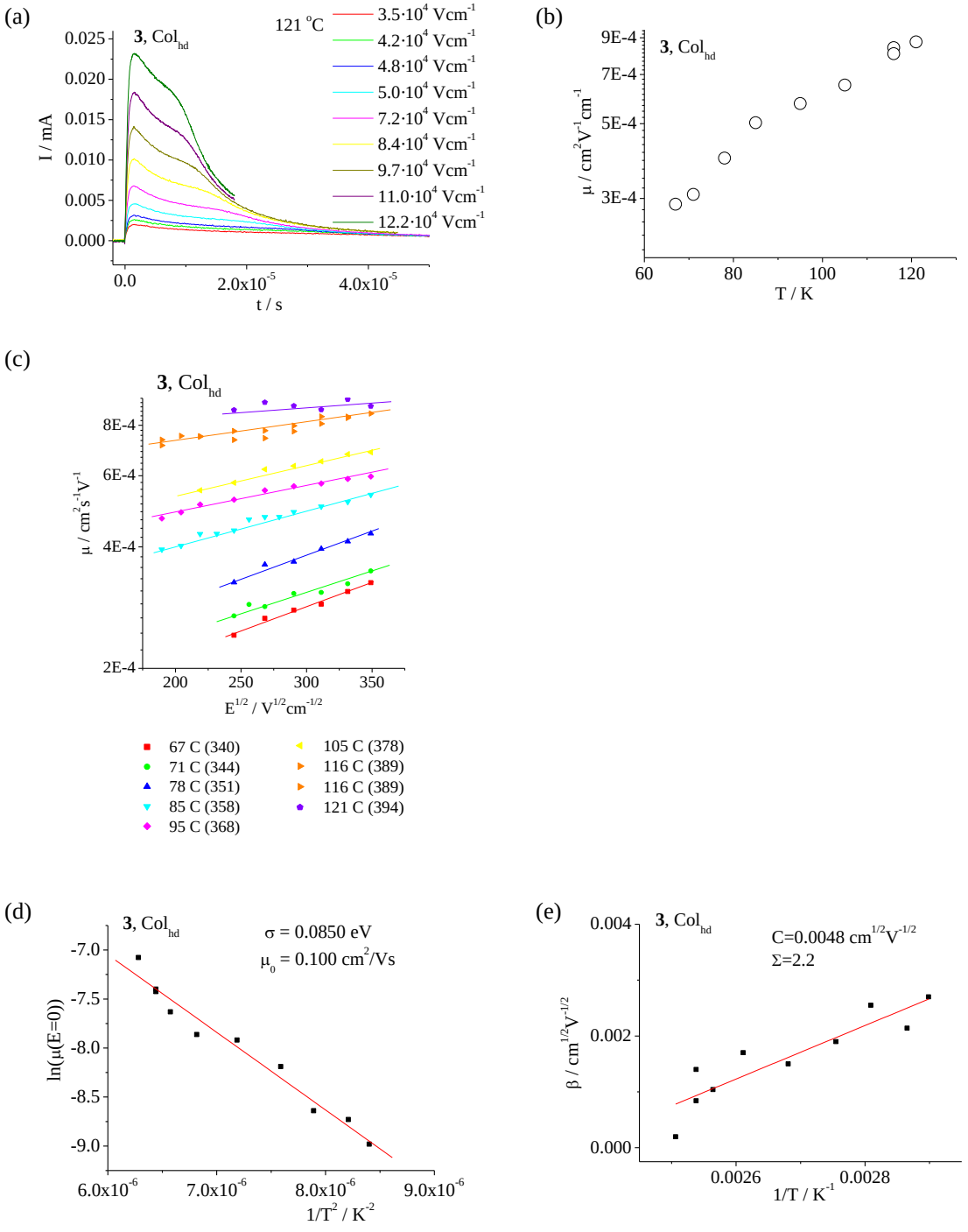

Figure SI7. Data compound **3:** (a) TOF transients current of holes for Col$_{hd}$ phase at constant temperature (121 °C) for different values of applied electric field (b) Temperature dependence of hole mobility at constant electric field (9.7 · 10^4 V/cm) in Col$_{hd}$ phase. (c) Field dependence of hole mobility (Poole-Frenkel relation) in Col$_{hd}$ phase. (d) Zero-field hole mobility and (e) slope β of the $\ln\mu(E^{1/2})$ dependence given in (c), $\beta = C[(\sigma/kT) - \Sigma]$.

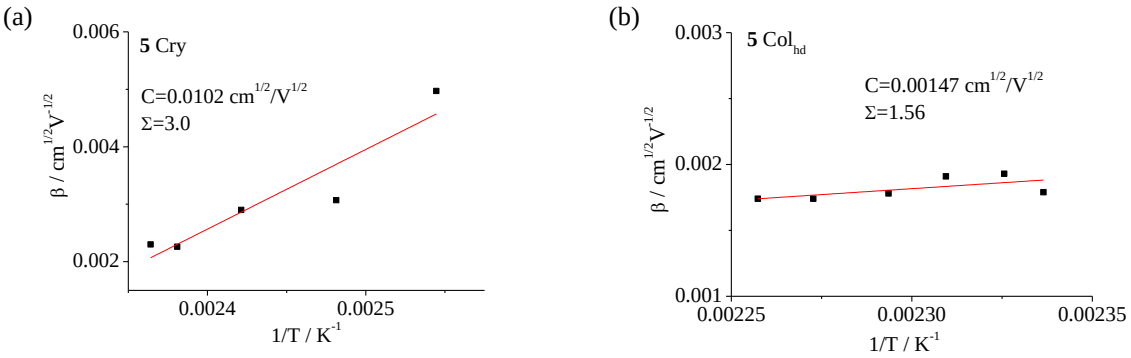

Figure SI8. (a) Data for compound **5**: Slope β of the $\ln\mu(E^{1/2})$ dependence given in Figs. 5a and 5b (main text), $\beta = C[(\sigma/kT) - \Sigma]$.

References

1. J. E. Foster, C. Lavigueur, Y-C. Ke and V. E. Williams, *Journal of Materials Chemistry* 2005, **15**, 4062.
2. G. A. Crosby and J. N. Demas, *Journal of Physical Chemistry*, 1971, **75**, 99
3. P. M. Borsenberg, L. Pautmeier and H. Bässler, *Journal of Chemical Physics*, 1991, **95**, 1258.